Journal of Alzheimer's Disease 58 (2017) 841–853
DOI 10.3233/JAD-170136
IOS Press

In Vivo Detection of Gray Matter Neuropathology in the 3xTg Mouse Model of Alzheimer's Disease with Diffusion Tensor Imaging

Wanda M. Snow[a,b,*], Ryan Dale[a,b], Zoe O'Brien-Moran[c], Richard Buist[d], Danial Peirson[a,b], Melanie Martin[b,c,d] and Benedict C. Albensi[a,b,*]
[a]*Division of Neurodegenerative Disorders, St. Boniface Hospital Albrechtsen Research Centre, Winnipeg, MB, Canada*
[b]*Department of Pharmacology & Therapeutics, University of Manitoba, Winnipeg, MB, Canada*
[c]*Department of Physics, University of Winnipeg, Winnipeg, MB, Canada*
[d]*Department of Radiology, University of Manitoba, Winnipeg, MB, Canada*

Accepted 22 March 2017

Abstract. A diagnosis of Alzheimer's disease (AD), a neurodegenerative disorder accompanied by severe functional and cognitive decline, is based on clinical findings, with final confirmation of the disease at autopsy by the presence of amyloid-β (Aβ) plaques and neurofibrillary tangles. Given that microstructural brain alterations occur years prior to clinical symptoms, efforts to detect brain changes early could significantly enhance our ability to diagnose AD sooner. Diffusion tensor imaging (DTI), a type of MRI that characterizes the magnitude, orientation, and anisotropy of the diffusion of water in tissues, has been used to infer neuropathological changes *in vivo*. Its utility in AD, however, is still under investigation. The current study used DTI to examine brain regions susceptible to AD-related pathology; the cerebral cortex, entorhinal cortex, and hippocampus, in 12-14-month-old 3xTg AD mice that possess both Aβ plaques and neurofibrillary tangles. Mean diffusivity did not differ between 3xTg and control mice in any region. Decreased fractional anisotropy ($p < 0.01$) and axial diffusivity ($p < 0.05$) were detected only in the hippocampus, in which both congophilic Aβ plaques and hyperphosphorylated tau accumulation, consistent with neurofibrillary tangle formation, were detected. Pathological tau accumulation was seen in the cortex. The entorhinal cortex was largely spared from AD-related neuropathology. This is the first study to demonstrate DTI abnormalities in gray matter in a mouse model of AD in which both pathological hallmarks are present, suggesting the feasibility of DTI as a non-invasive means of detecting brain pathology *in vivo* in early-stage AD.

Keywords: 3xTg, Alzheimer's disease, diffusion tensor imaging, gray matter, hippocampus, neurofibrillary tangles

INTRODUCTION

Alzheimer's disease (AD) is a neurodegenerative disorder clinically characterized by severe cognitive and functional impairment, including difficulty in forming new memories. Anatomically, AD is characterized by extensive neuropathology, including the accumulation of amyloid-β (Aβ) and its aggregation into fibrillar plaques as well as the hyperphosphorylation of tau protein, resulting in intracellular neurofibrillary tangles. Structural brain changes also occur, including significant atrophy and neuronal loss. Although diagnostic criteria have been recently updated in efforts to improve diagnostic accuracy, including the recommended use of biomarkers

*Correspondence to: Dr. Benedict C. Albensi and Wanda M. Snow, St. Boniface Hospital Research, Division of Neurodegenerative Disorders, 351 Tache Ave/R4050, Winnipeg, MB R2H 2A6, Canada. Tel.: +1 204 235 3941; Fax: +1 204 237 4092; E-mail: wsnow@sbrc.ca/wsnow 2001@yahoo.ca (W.M. Snow) and Tel.: +1 204 235 3942; Fax: +1 204 237 4092; E-mail: balbensi@sbrc.ca (B.C. Albensi).

ISSN 1387-2877/17/$35.00

(e.g., positron emission tomography to detect Aβ or hypometabolism), there is no biomarker that has been consistently validated for use across the AD spectrum [1]. At present, a diagnosis of AD can only be definitively confirmed by neuropathological exam at autopsy and is indicated by the presence of Aβ plaques and neurofibrillary tangles [2]. Structural magnetic resonance imaging (MRI) has detected brain and regional volumetric changes in AD *in vivo*, with hippocampal volume being the most consistent imaging biomarker for AD [3]. By the time hippocampal volume is altered and detectable with current imaging protocols, however, significant and irreversible neuronal loss has occurred. Further, decreased brain volume precedes neurocognitive symptoms in AD by years [4]. Thus, there is considerable effort to develop *in vivo* antemortem diagnostic measures of AD that can be used for early detection, where therapies to halt the disease will be most valuable.

Diffusion-based MRI offers promise as a means of early diagnosis of AD. Diffusion tensor imaging (DTI) can measure the diffusion of water molecules through tissue in multiple orientations, and, hence, the directionality and magnitude of water diffusion. DTI scans derive directional information using 3D or multidimensional vector algorithms based on six or more gradient directions, which allows one to compute the diffusion tensor. Thus, DTI is often used to assess white matter integrity, as water in white matter follows an anisotropic, or highly directional, diffusion pattern due to physiological constraints to diffusion placed by axonal membranes, etc. (see [5] for review). The parameter fractional anisotropy (FA) is a measure of the relative degree of directionality of water diffusion and can range from 0 (indicative of isotropic motion) to 1 (indicative of anisotropic, or directional, diffusion). FA has been used to probe white matter in AD, with reports consistently demonstrating decreased FA (i.e., more random diffusion) values that are assumed to result from degradation to myelinated fibers through Wallerian degeneration or via mechanisms independent of gray matter neurodegeneration [6].

Although less studied, DTI has also been exploited to measure microstructural alterations in gray matter indirectly in AD. For example, DTI has been shown to differentiate AD patients from cognitively healthy controls with accuracy rates on par with gray matter volume estimates obtained using structural MRI [7]. In fact, some studies [8] found no predictive value in volumetry data for conversion to AD from its prodrome, mild cognitive impairment (MCI), in the short-term (2 years), whereas DTI measures were predictive. Diffusivity in the hippocampus, a key region for memory formation that is particularly susceptible to AD-related neurodegeneration [9], may predict progression from MCI to AD more accurately than hippocampal atrophy measured by structural MRI [10, 11]. Although other studies in humans failed to show significant diffusivity differences between MCI and AD [12], the diagnostic utility of DTI in AD was supported in a recent meta-analysis, with a greater effect size detected for changes in hippocampal diffusivity measures than volumetry [13]. Typically, DTI studies of gray matter measure mean diffusivity (MD), an indication of the overall magnitude of water diffusion that is independent of direction. Specifically, increased MD has been reported in the hippocampi of: 1) MCI patients versus healthy age-matched controls [10], 2) MCI patients who converted to AD versus those who did not [14, 15], 3) AD versus MCI patients [16, 17], 4) AD patients versus healthy age-matched controls, and 5) AD patients versus those with another common type of dementia, dementia with Lewy bodies [18]. Further, increased hippocampal MD better predicts impaired verbal memory in MCI patients than decreased hippocampal volume [10].

In addition to the hippocampus, MD is also elevated in other brain regions in those with AD versus healthy controls or MCI controls, including entorhinal cortex [19], temporal [19], parietal [8, 19], frontal [19], and occipital lobe regions [8] as well as lateral temporal and parietal lobe association cortices [18]. Such findings of increased MD are assumed to result from the degeneration of physiological barriers to diffusion (i.e., reduced cellular membrane in neurons from stunted axons and dendrites, neuron loss) [20, 21]. Although neuronal loss and subsequent brain atrophy that accompany AD would be expected to decrease the physiological barriers to water diffusion, the presence of both intra- and extracellular protein deposits (i.e., Aβ plaques and neurofibrillary tangles) may be expected to decrease MD in the AD-like brain. Although DTI measures can infer pathological alterations in the brain, it cannot differentiate micro- from macrostructural abnormalities, nor can it confirm the underlying pathology causing the distinct diffusional behavior in AD.

Although MD is a common parameter to assess gray matter using DTI, FA has also been used but to a much lesser degree. Unlike MD, which is increased, the few studies to date have shown reduced

hippocampal FA in DTI studies in both MCI [10] and in AD [12] relative to controls. Further, hippocampal FA values were predictive of verbal memory in MCI patients [10].

To enhance our understanding of the relationship between diffusivity changes and brain pathology in the context of AD, DTI has been used in mouse models of AD and AD-related pathology, where neuropathological changes can be confirmed post-imaging. In PDAPP mice, characterized by overexpression of human amyloid-β protein precursor (AβPP) and subsequent Aβ plaque formation, little change was detected in axial diffusivity (AxD), a measure of diffusivity along the principal direction that is used to calculate FA, whereas radial diffusivity (RadD), a measure of diffusivity perpendicular to the principal direction of diffusion, increased in white matter [22]. Gray matter was not evaluated, however. In the Tg2576 or APPsw line, which exhibit Aβ plaque deposition, AxD was reduced in several white matter tracts. In gray matter, the trace of the diffusion tensor was decreased in both hippocampal and cortical tissue [23]. In contrast, in TgCRND8 mice, also characterized by robust Aβ plaque deposition, no differences in diffusivity were detected in hippocampal or cortical tissue using diffusion weighted imaging [24]. Studies of double transgenic APP/PSI mice [25, 26], in which both Aβ plaque deposition and neuron loss occur, report elevated diffusivity measures in multiple brain regions, including gray matter-rich hippocampus and cortex.

Although these aforementioned studies help to elucidate the potential role of diffusion-based MRI as a means of detecting microstructural differences in the AD-like brain, they tell us little about diffusivity behavior in the presence of a key hallmark of AD, neurofibrillary tangles. More recently, an increase in the mobility of water around paired helical filaments of tau relative to tau monomers was reported, with the authors speculating that this phenomenon could underlie enhanced MD reported in AD [27]. At present, no DTI studies have been carried out using a model of AD that possesses tau pathology, where histochemical confirmation could be carried out post-imaging. The triple transgenic (3xTg) AD mouse exhibits several age-dependent hallmarks of the disorder, including the presence of both brain Aβ plaques and neurofibrillary tangles as well as memory deficits [28]. Assessment of white matter in 3xTg mice using DTI revealed no significant differences between age-matched controls [29]. Whether microstructural abnormalities in gray matter in this common AD model can be detected using DTI, however, has not been determined. To explore the potential utility of DTI further as a means of detecting gray matter neuropathology in early-stage AD and to examine these parameters specifically in the presence of confirmed tau pathology, we examined various DTI metrics in 3xTg mice at 12-14 months, shortly after plaque deposition and neurofibrillary tangles occur in a region- and age-dependent manner [30]. Mice of this age are considered middle-aged, corresponding to humans approximately in their fourth decade [31]. Therefore, this age range was chosen to investigate DTI as a means of detecting AD-related neuropathology in the middle-aged mammalian brain, an age range that is typically prior to AD diagnoses.

MATERIALS AND METHODS

Animals

A total of 15 3xTg ($n = 7$) and age-matched control ($n = 8$) background mice (C57BL/6) of male and female sex underwent MRI at 12–14 months. These methods were approved by the institutional Animal Care Committee, which adheres to guidelines set forth by the Canadian Council on Animal Care. The 3xTg strain, originally a gift from Dr. Mark Mattson (National Institutes of Health, Baltimore, Maryland), was maintained on a C57BL/6 background for eight generations. Both 3xTg and control mice were bred and aged at the institution. Mice were provided with food and water *ad libitum* and maintained on a 12-h light/dark cycle.

MRI data acquisition

Animals were anaesthetized with inhaled isoflurane (5.0% for induction, 2.0–2.5% for maintenance) in a mixture of 30:70 O_2:N_2O and maintained in position using a nose cone with attached bite bar. Respiration rate was monitored and maintained between 40–100 breaths/minute with an electronic small-animal monitoring and gating system (Small Animal Instruments, Inc., Stony Brook, NY, USA). Body surface temperature of animals was maintained at 37.0°C with a fluid-filled heating pad connected to a water bath. Total time under anesthetic during preparation and *in vivo* scanning for each animal was approximately 75 min.

Animals were scanned in a Bruker Avance III horizontal bore small-animal MRI at 7.0T using

Paravision 5.0 acquisition software (Bruker BioSpin, Ettlingen, Germany). Rapid-acquisition with relaxation enhancement (RARE) T_2-weighted imaging was performed to produce reference images using the anterior horn of the corpus callosum as a visible landmark for placement of the first slice (TR: 1640 ms, TE: 80.0 ms, image matrix: 256×256, FOV 3.0 cm $\times$ 3.0 cm, 117×117 μm^2, slice thickness: 1.0 mm, slices: 3, acquisition time: 10 min 29 s). Multi-shot echo planar imaging (EPI) was used to improve acquisition efficiency for DTI with an orthogonal six direction gradient scheme (b-value: 1000 s/mm^2, gradient duration 3 ms, gradient separation 15 ms, TR: 1250 ms, TE: 26.6 ms, 4 EPI shots, 32 averages, image matrix: 128×96 auto-filled to 128×128, FOV: 3.0 cm $\times$ 3.0 cm, in plane resolution: 234×234 μm^2, slice thickness: 1.0 mm, slices: 3, acquisition time: 24 min).

Image reconstruction was performed in MATLAB (Natick, MA, USA). Prior to fitting the tensor, the diffusion weighted images (DWIs) were registered to the "b = 0" image using rigid affine transformations. The diffusion tensor "D" was used to quantify anisotropic diffusion. D was estimated from six DWIs in addition to a "b = 0" measurement and was represented by a 3×3 matrix [32]. D was first estimated using a linear least-squares (LLS) fit [32, 33]. The tensor was then weighted to account for noise in the image and the consequent uncertainties in the tensor values [34]. The data were scaled using Salvador weights ($w = (S/\sigma)^2$) [35] such that more weight was given to measurements with higher signal strength and less noise. Lastly, the tensor was constrained to be positive-definite to ensure physical relevance [36]. Similar calculations and fits were used in our previous studies [37].

Once D was estimated for each voxel, the matrices were diagonalized to determine eigenvalues and eigenvectors. The tensor eigenvalues were used to calculate the scalar metrics used in diffusion analysis (MD, FA, RadD, AxD). The principal eigenvector and the FA metric were used to produce the 24-bit directionally encoded color map (DEC) to represent direction and degree of anisotropic diffusion in brain structures. DTI slices were oriented to bregma (defined below) during acquisition.

Region-of-interest (ROI) analyses were performed to detect changes in the entorhinal cortex, the hippocampus, and the cortex (including motor and somatosensory cortex) as well as the whole brain section. The ROIs were delineated in the DEC with reference to the Allen Mouse Brain Atlas [38] (http://mouse.brain-map.org) and others [39] and included the entorhinal cortex (at the level of –4.20 mm to bregma), the hippocampus (at the level of –2.20 mm to bregma), and the cortex (at the level of –0.2 mm to bregma). The ROIs were applied to all quantitative scalar maps, and scalar metrics were averaged.

Amyloidogenic plaque staining with Congo red

After *in vivo* scanning, histological examination of neuropathology was conducted in the three ROIs in a subset of mice ($n = 2$–4). Brain sections were obtained from the same bregma coordinates as those used for DTI measures. Detection of amyloidogenic deposits was done using Congo red staining, considered the gold standard for detecting Aβ deposits at autopsy [40]. Following MRI, brain tissue was dissected, immersed in paraformaldehyde (4%), frozen with cooled isopentane, and stored at –80°C. Frozen tissue was cryosectioned to a thickness of 10 μm, collected onto Microfrost slides, air-dried (room temperature), and stored at –20°C until staining. Aβ plaques were stained according to a protocol kindly provided by Dr. Glenys Tennent (University College London) based on the Puchtler method [41]. Briefly, sections were rehydrated in phosphate-buffered saline, pH 7.4, for 5 minutes, followed by immersion in Mayer's hematoxylin for 3.5 minutes to counterstain nuclei. After rinsing in running cold tap water (5 min), sections were pretreated in an alkaline alcoholic-saturated sodium chloride solution (80% EtOH + NaCl (2%) + 0.01% NaOH) for 20 min, followed by immersion in alkaline alcoholic Congo red solution saturated with NaCl (0.2% Congo red in 80% EtOH + NaCl (2%) + 0.01% NaOH). Sections were then dehydrated in absolute ethanol (3 washes), cleared with Xylene (2×5 min), and coverslipped with Permount (Fisher Scientific, Waltham, MA, USA). Sections were viewed with a Nikon Eclipse TE200 microscope. Brightfield images were captured with an Infinity 2-1R CCD camera (Lumenera Corp., Ottawa, Ontario, Canada).

Neurofibrillary tangle staining with immunohistochemistry

After removal from –20°C-storage, cryosections (10 μm) were air-dried for 60 min and washed in 1X Tris-buffered saline with 0.1% Tween 20 (TBS-T) (5 min). As neurofibrillary tangles are comprised of paired helical tau filaments that are in a

hyperphosphorylated state, neurofibrillary tangle formation was detected with AT180 mouse monoclonal antibody (against paired helical filamentous tau; cat. No. MN1040, ThermoScientific, Rockford, IL, USA; overnight at 4°C at 1:100 dilution) in conjunction with the EXPOSE HRP/DAB Detection IHC Kit (Abcam, Cambridge, Massachusetts, USA). The manufacturer's protocol was followed with the addition of a 1-h incubation with 10% goat serum and F(ab) fragment of unconjugated goat anti-mouse IgG (Jackson Laboratories; 1:10 dilution) in TBS-T prior to primary antibody incubation to prevent background staining due to the use of a mouse primary antibody for detection in mouse tissue. Tissue sections from 3xTg hippocampus in which the primary antibody was omitted during incubation served as negative controls.

Statistical analyses

Means and standard deviations were computed for each ROI and for the whole slice. MRI data were subjected to tests of normality and homogeneity of variance, followed by the Student's *t*-test of means or the non-parametric Mann-Whitney U test as appropriate. All analyses were conducted with SPSS v20 (IBM Corp., Armonk, NY, USA). All statistical tests were two-tailed, and statistical significance was set at $p < 0.05$.

RESULTS

DTI measures

After manual segmentation of ROIs from the DEC maps (see Fig. 1), diffusional parameters were measured. No significant differences ($p > 0.05$) were found in any of the diffusivity metrics in the cortex, entorhinal cortex, or in the corresponding brain slices in their entirety. Significant differences between 3xTg and control mice were detected, however, in metrics in the hippocampus. FA was reduced by 33% ($p = 0.01$) in 3xTg hippocampus and by 25% overall in the brain slice containing the hippocampus ($p < 0.01$) relative to values from control mice, indicating less anisotropic diffusion and, hence, greater isotropic diffusion of water in this brain region in 3xTg mice. AxD was reduced by nearly 17% in the 3xTg hippocampus as compared to the same region in age-matched controls ($p < 0.05$). In the slice containing the hippocampus, RadD was significantly increased by 10% in 3xTg mice ($p < 0.05$). MD was not significantly different in any region examined (see Table 1).

Histology

To confirm neuropathology in the 3xTg hippocampus, in which DTI measures were altered, Congo red and immunohistochemical staining of Aβ plaques and pathological tau, respectively, were performed in a subset of mice that underwent scanning. No congophilic plaques were detected in the entorhinal cortex of either 3xTg or age-matched control mice (Fig. 2A, B). Tau-positive neurons were not present in the entorhinal cortex of control or 3xTg mice, however intense staining was present in the adjacent subiculum (Fig. 2C, D). In the hippocampus of age-matched wild-type C57BL6 controls, no Aβ plaques were found (Fig. 2E), whereas parenchymal Aβ plaques were detected in the hippocampi of 12-14-month-old 3xTg mice, as evidenced by pink-red congophilic deposits (Fig. 2F). Immunoreactivity for hyperphosphorylated tau was detected in hippocampal tissue in 3xTg mice, with extensive staining in the CA1 region relative to a lack of immunoreactive neurons in control hippocampus (Fig. 2G, H). In the cortex, no congophilic plaques were detected in 3xTg or their wild-type controls (Fig. 2I, J). Several neurons in the 3xTg cortex, however, demonstrated immunoreactivity for pathological tau but to a less intense degree than seen in the 3xTg hippocampus (Fig. 2L). There was an absence of immunoreactivity against pathological tau in control cortical tissue (Fig. 2K). Negative control sections without primary antibody added to the incubation solution were devoid of tau-positive neurons (not shown).

DISCUSSION

The present study examined diffusivity behavior in several gray matter regions known to be affected in AD in symptomatic mice from a common and relevant AD model, the 3xTg strain. Of the three regions studied, only the hippocampus exhibited altered diffusivity metrics, including decreased FA and AxD. In conjunction with altered DTI parameters, the hippocampus was the only ROI studied in which both pathological markers of AD, amyloid plaques and neurofibrillary tangles, were present. To our knowledge, this is the first study to investigate DTI as a means of assessing microstructural gray matter changes *in vivo* using a model of AD that

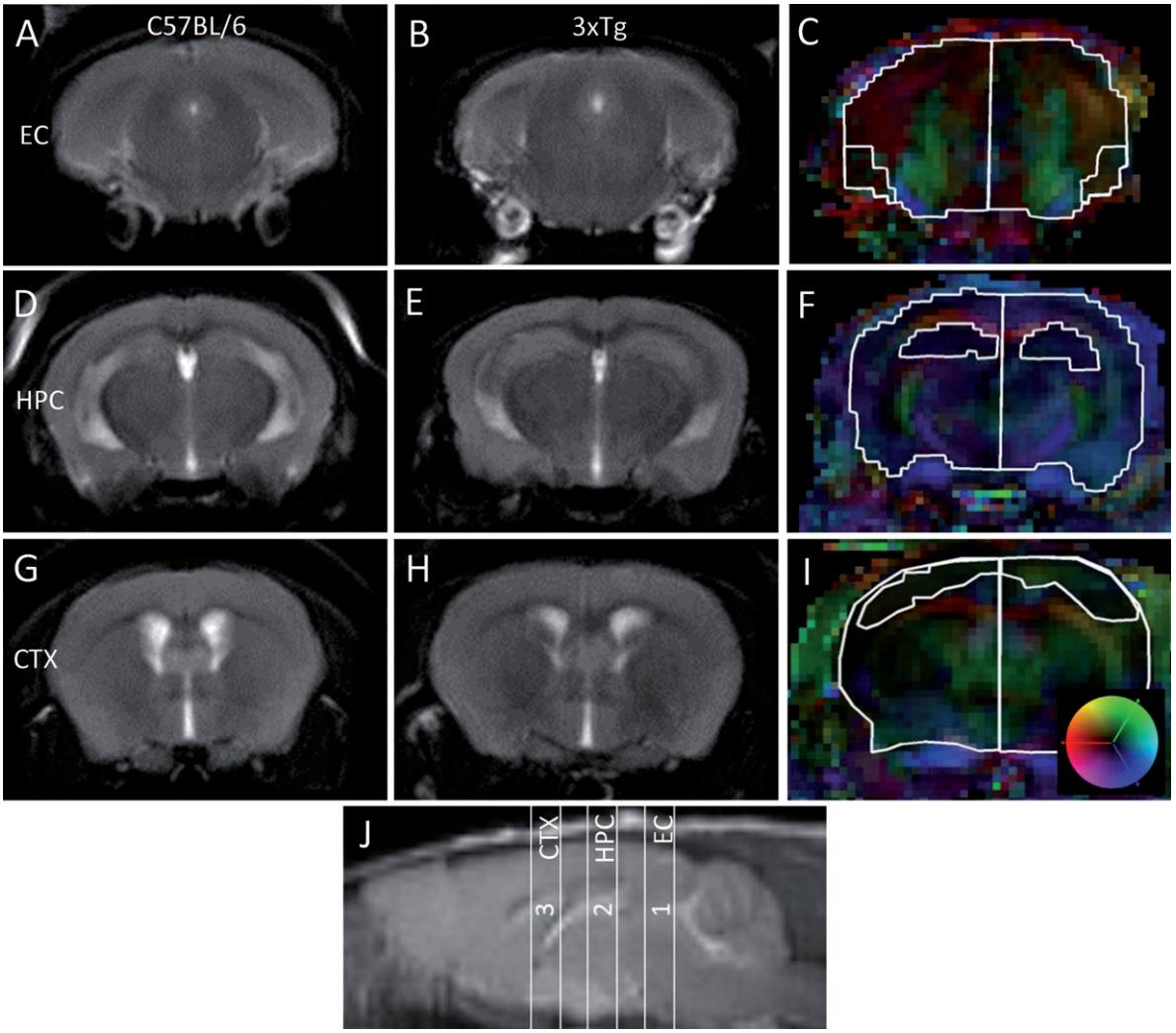

Fig. 1. Sample RARE images and ROI determinations of gray matter structures in C57BL/6 and 3xTg for DTI analyses. ROIs were manually segmented in DEC maps using a custom-built Matlab gui [37], with reference to the Allen Mouse Brain Atlas [38] and to the work of Borg and Chereul (2008). A-C) Slice 1 – Entorhinal Cortex (EC): RARE (A, B) and ROI (C) at the level of –4.20 mm to bregma, including the EC (inner trace) and whole slice (outer trace). D-F) Slice 2 – Hippocampus (HPC): RARE (D, E) and ROI (F) at the level of –2.20 mm to bregma, including the HPC (inner trace) and whole slice (outer trace). C-I) Slice 3 – Cortex (CTX): RARE (G, H) and ROI (I) at the level of –0.2 mm to bregma, including the CTX (inner trace) and whole slice (outer trace). Color map in (I) indicates the directions of the primary diffusion in each voxel for (C), (F), and (I); red indicates right-left, green indicates head-foot, and blue indicates anterior-posterior from 0 (center) to 1. J) RARE image in the sagittal orientation indicating position of slices (numbered) from which ROIs were segmented.

encompasses both cardinal neuropathological hallmarks of Aβ plaques and neurofibrillary pathology. Although MD was not altered, as has been consistently reported in MCI and AD, the current findings of reduced FA in the 3xTg model relative to controls are in line with human DTI of both conditions [10, 14].

Interestingly, initial characterizations of the 3xTg strain demonstrated that unlike Aβ plaques, which initiate in the cortex at 6 months and progress to the hippocampus, tau pathology appears in the hippocampus first at 12 months, with progression to the cortex later [30]. In contrast, mice in the present study did not exhibit robust amyloid plaque deposition in the cortex nor in the entorhinal cortex. Other labs have reported a lack of extracellular Aβ deposits despite evidence of tau pathology in the brains of 3xTg mice at the age used in the present study [42], as well as in old mice (22 months) [43]. Such variability in pathology amongst animals from different laboratory colonies and from initial reports characterizing this transgenic AD strain argue

Table 1
Mean (±standard deviation) DTI parameters in gray matter in 12–14 month-old 3xTg versus C57BL/6 control mice

ROI/DTI metric	3xTg ($n=7$)	Control ($n=8$)	p
Entorhinal Cortex			
MD	1.01 ± 0.25	0.90 ± 0.09	0.3
RadD	0.73 ± 0.13	0.72 ± 0.07	0.9
AxD[#]	1.58 ± 0.92	1.27 ± 0.27	0.4
FA	0.40 ± 0.22	0.38 ± 0.14	0.8
Hippocampus			
MD	0.94 ± 0.05	1.00 ± 0.15	0.2
RadD	0.85 ± 0.04	0.85 ± 0.15	0.9
AxD	1.14 ± 0.09	1.37 ± 0.02	0.02*
FA	0.22 ± 0.04	0.33 ± 0.09	0.01*
Cortex			
MD	0.86 ± 0.12	0.83 ± 0.22	0.7
RadD	0.72 ± 0.16	0.68 ± 0.19	0.7
AxD	1.14 ± 0.14	1.12 ± 0.34	0.9
FA	0.31 ± 0.17	0.33 ± 0.14	0.8
Slice 1 with Entorhinal Cortex			
MD	1.05 ± 0.28	0.95 ± 0.11	0.4
RadD	0.73 ± 0.11	0.75 ± 0.08	0.7
AxD	1.68 ± 0.99	1.34 ± 0.29	0.4
FA	0.43 ± 0.20	0.38 ± 0.13	0.6
Slice 2 with Hippocampus			
MD	0.99 ± 0.06	0.96 ± 0.09	0.5
RadD	0.85 ± 0.05	0.77 ± 0.07	0.045*
AxD	1.27 ± 0.08	1.33 ± 0.16	0.4
FA	0.28 ± 0.03	0.37 ± 0.06	0.004**
Slice 3 with Cortex			
MD	0.95 ± 0.11	0.95 ± 0.11	1.0
RadD	0.78 ± 0.13	0.78 ± 0.11	0.9
AxD	1.27 ± 0.12	1.29 ± 0.20	0.8
FA	0.33 ± 0.12	0.35 ± 0.11	0.8

MD, RadD, and AxD are in units of 10^{-3} mm^2/second. FA is a ratio and, therefore, has no units. *$p<0.05$; **$p<0.01$, as analyzed by Student's t-test or [#]Mann-Whitney U.

for confirmation of neuropathological findings, as done here, in studies using this strain. The lack of detectable differences in DTI metrics in the cortex, in which several tau-positive neurons were evident, coupled with the altered metrics found in the hippocampus, which demonstrated both plaques and tangles, suggests for a primary contribution of the plaque deposition to the DTI signal reported here, or possibly the combination of the two pathological features. Consistent with this interpretation is the finding of a the lack of DTI differences in the slice containing the entorhinal cortex, in which immunoreactivity for pathological tau was particularly intense in the subiculum, as previously reported [29, 44, 45]. Using diffusion weighted imaging, however, TgCRND8 mice failed to show altered diffusivity in gray matter regions, including the hippocampus and cerebral cortex [24], regions with robust plaque deposition in the absence of neurofibrillary tangles, suggesting it is the co-occurrence of both Aβ plaques and neurofibrillary tangles that contributes to the altered DTI measures in the present study. One must exercise caution in interpreting results of DTI because changes in DTI metrics reflect differences in the diffusion behavior of water and thus imply some sort of neuropathology. They cannot, however, speak to the specific neuropathology and/or microstructural changes, alone or in combination, that result in any observed diffusivity changes. Because of the clear directionality of water diffusion in the white matter along axonal bundles, DTI is often used to assess white matter anatomy with a reliance on directional data (i.e., FA). A consistent finding in AD is an increase in MD [5] with a concomitant decrease in FA, with the majority of studies that report such differences in FA examining white matter. ROI-based DTI studies report decreased FA in several white matter tracts in AD, including the fornix [46, 47], corpus callosum [48–50], and cingulum bundle [51–53] (as reviewed in [21]) similar to reduced FA indices reported here in 3xTg hippocampus. Interestingly, a previous DTI study of 3xTg mice [29] did not detect any differences in white matter pathology, as reported in AD.

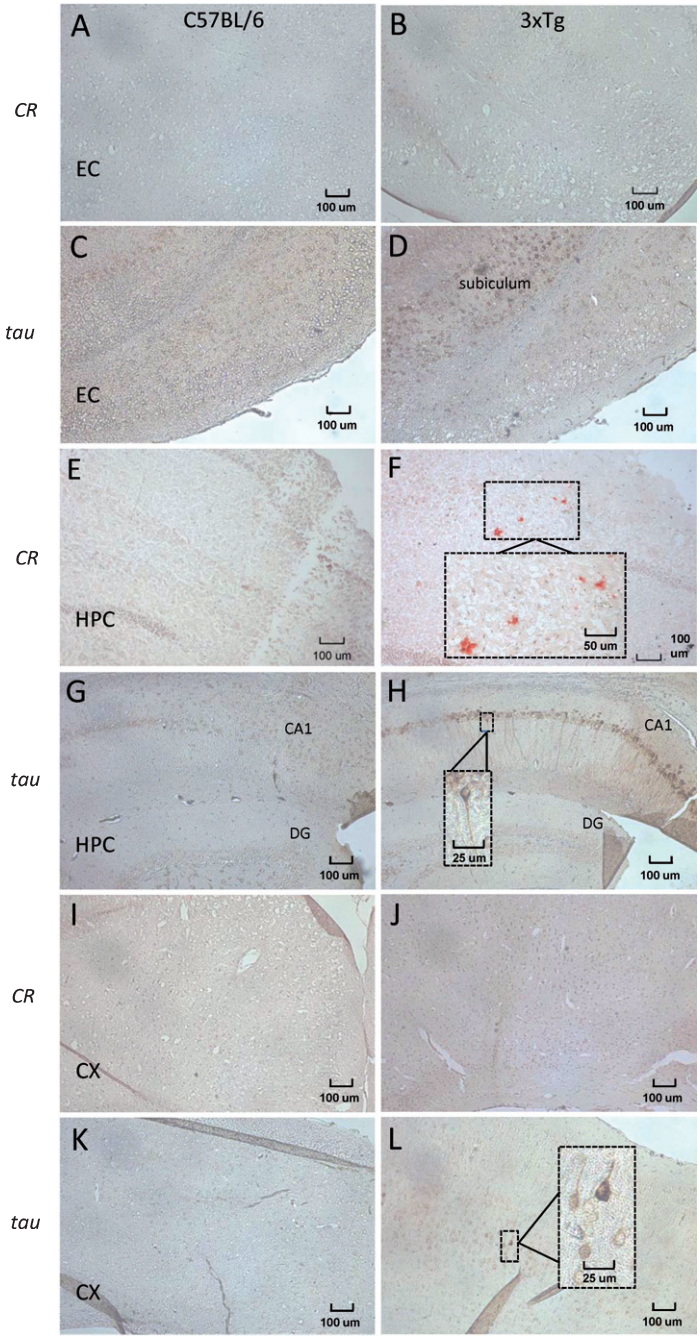

Fig. 2. Representative brightfield images of Aβ plaque deposition and neurofibrillary tangle formation in cryosections (10 μm) taken from the ROIs of 12–14 month 3xTg and age-matched C57BL/6 control mice. Congo red (CR) staining was used to visualize Aβ plaque deposition, and immunohistochemistry for hyperphosphorylated tau (MN1040 antibody) was used to detect neurofibrillary tangles. A, B) No congophilic plaques were detected in the entorhinal cortex (EC) of either control (A) or 3xTg (B) mice. Immunohistochemistry for hyperphosphorylated tau did not detect tau-positive neurons in the EC of control (C) or 3xTg mice, although immunoreactivity (brown staining) was high in the subiculum adjacent to the EC in transgenic mice (D). Sections from control hippocampus (HPC) did not contain evidence of Aβ plaques (E), whereas several red congophilic deposits were apparent in the HPC of 3xTg mice (F). Immunoreactivity for tau was weak in sections containing the CA1 and dentate gyrus (DG) of the HPC in control mice (G). In 3xTg tissue, extensive staining was noted in several neurons along the corresponding CA1 region, with a lack of staining in the DG (H). The cortex (CX) of both control (I) and 3xTg (J) brains were devoid of congophilic plaques. Relative to the lack of immunoreactivity for hyperphosphorylated tau in control CX (K), several neurons in the 3xTg CX exhibited positive staining (L). Images magnified 100x, with boxed inserts (F, H, L) magnified 400x.

In gray matter, FA is generally low due to the more unstructured array of cellular membranes and processes as compared to white matter regions, in which there is significant directional preference along the axis of axons within fibre tracts [54]. In contrast to FA, MD represents the overall magnitude of diffusivity in all directions measured, and, therefore, is more reflective of spatial properties of the tissue rather than of a bias in any particular direction [55]. Hence, MD is often examined in studies of gray matter [21].

In AD, reports of increased MD are typical in areas associated with significant neuronal loss, including the hippocampus [18], entorhinal cortex [19], and temporo-parietal association cortex [18]. In mice, increased MD, FA, AxD, and RadD were found in an experimental model of forebrain cholinergic neuron loss that mimics AD-related forebrain pathology [56]. Here, DTI metrics were found to correlate inversely with forebrain cholinergic neuron loss. Diffusivity parameters, however, were collected *ex vivo* on fixed tissue [56].

Only a handful of studies have investigated brain diffusivity changes *in vivo* in AD models. DTI studies in APP/PS1 mice, a more severe phenotype with Aβ plaque deposition and marked neuron loss, report significant increases in multiple parameters (i.e., MD, FA, AxD, RadD) in several gray matter regions, including hippocampus and cortex [25, 26]. In the same strain, Zerbi et al. [57] found similar results, with increased MD, AxD, and RadD in the hippocampus. Moreover, in mice with a 25% reduction in forebrain cholinergic neurons, mimicking the preferential loss of cholinergic neurons in AD, forebrain diffusivity is increased, with higher MD, FA, AxD, and RadD measures relative to controls [56]. In contrast, a study by Sun et al. [23] in APPsw mice, which display a mild AD phenotype characterized by plaque deposition in the absence of other neuropathological characteristics of AD (e.g., tangles or neuron loss), found a decrease in the trace of the diffusion tensor, a directionally averaged diffusion coefficient. No other diffusivity metrics, however, were analyzed in gray matter. Surprisingly, DTI measures did not correlate strongly with Aβ load [23]. In another study in APP mice, whole brain-based DTI analysis also found decreased MD in gray matter regions, including the amygdala and hippocampus [58]. Thus, DTI studies of AD models with marked neuron loss indicate increased MD, whereas those of a more mild neuropathological phenotype without neuron loss (e.g., APP) tend to report decreased MD or, in the case of 3xTg, no change in MD in gray matter. Such results are consistent with an interpretation of increased freedom of water molecules to diffuse in less neuron-dense and membrane-packed brain parenchyma. Accordingly, the overall magnitude of diffusivity (e.g., MD) was not significantly altered in gray matter regions in 3xTg mice in the present study, consistent with preserved neuronal density in the 3xTg model relative to AD and other mouse models. Our results, however, are in contradiction to several of the aforementioned DTI findings in mouse models of AD [25, 26, 56] in that FA was decreased in gray matter in 3xTg mice. A notable distinction between the 3xTg model used in the present study and other models is the presence of neurofibrillary tangles in the 3xTg brain, which may account for some of the discrepancies. The study by Muller et al. [58], however, also reported decreased FA and AxD in the hippocampus, consistent with the present findings, as well as the entorhinal cortex, in old (23-month) APP mice in the absence of neurofibrillary tangle pathology. The 3xTg model is well-suited to investigate the potential contribution of tau pathology to DTI metrics related to AD, as this model possesses both Aβ plaques and neurofibrillary tangles without significant neuron loss, thereby allowing for an investigation of tau-related diffusivity without the potential confounds of neuron loss, which would be expected to impact MD. The presence of neurofibrillary tangles in the 3xTg hippocampus and cortex did not increase overall diffusivity (e.g., MD), as could be hypothesized based on recent findings of enhanced water mobility of paired helical filaments of tau that pathologically assemble in AD [27]. Future DTI studies in older mice in which Aβ deposition and neurofibrillary tangle formation is more extensive are warranted to more fully explore the relationship between DTI parameters in AD-related tau pathology.

Within the hippocampus, the current finding of a decrease in FA, a composite measure, is consistent with the individual measures of AxD and RadD, with a significant decrease in AxD and similar relative rates of RadD (e.g., FA = AxD / RadD). Therefore, decreased FA in 3xTg hippocampus comes from a corresponding decrease in AxD. Unlike other DTI studies in which MD and FA are the principal metrics examined, analysis of the individual components of FA (AxD and RadD), as present here, provides additional details regarding the precise alterations in diffusivity, as if both AxD and RadD are altered in proportion, FA will remain unchanged [59]. In the slice containing the hippocampus, however, the

reduced FA in 3xTg mice was driven by an increase in RadD, with no change in AxD.

Data suggest that AxD may be a more sensitive indicator of microstructural abnormalities in early-stage AD, whereas differences in RadD are detected in late-stage disease [5]. Increases in AxD may reflect some initiating early events, whereas changes in RadD may be more reflective of severe pathology, including neuron loss. These interpretations are consistent with our findings of pronounced changes in AxD but not RadD in the 3xTg hippocampus at 12–14 months of age, representative of early-stage AD without significant neuron loss. The present findings, however, are contradictory in the direction of the effect, as AxD decreased in the 3xTg hippocampus relative to age-matched controls in the present study. The fact that RadD was significantly increased in the slice containing the hippocampus with no difference in RadD in the hippocampal ROI itself is not due to a lack of power attributed to possibly an insufficient sample size, as the means were identical ($p = 0.9$) but rather suggests that areas surrounding the hippocampus in that region of the brain (–2.20 to Bregma) are affected in the 3xTg model. The slice in its entirety is more heterogeneous relative to the ROI generated in terms of biological material (e.g., ventricles, white matter) present that would be reflected in the diffusivity metrics. Although no significant differences have been detected in DTI metrics in 3xTg white matter [29], previous MRI studies have found enlargement of the lateral ventricles at both the cortical and hippocampal levels, with severe enlargement in the hippocampal region at 14 months [42]. This would be expected to contribute to altered diffusivity and could explain in part the increased RadD at the level of the hippocampus reported here. However, examination of the RARE images (Fig. 1) does not indicate any gross ventricular abnormalities in the 3xTg brain, as was apparent in the study by Hohsfield et al. [42].

Limitations and future studies

Although this study confirmed Aβ plaque deposition and hyperphosphorylated tau immunoreactivity, a measure of pathological tau, in the hippocampus in a subset of mice in which diffusivity was altered, a lack of available suitable samples prevented correlating neuropathological and DTI data. Such analyses would provide insight as to the degree of influence from each pathological feature on diffusivity behavior in the AD-like brain. Furthermore, given that 3xTg mice exhibit age-related neuropathology, future studies investigating how DTI metrics may change with age will also assist with elucidating what neuropathological features contribute to alterations in DTI measures. As well, a comparison of DTI metrics across multiple AD strains with varying pathologies would also help tease apart the contributions of various pathologies to specific DTI signals. Using a higher field strength imager, cryoprobes rather than traditional RF coils, and more diffusion encoding direction would allow for higher resolution studies of the brain to be collected in about the same amount of time as the images collected in this study [60]. This, in turn, would allow for a better comparison of DTI metrics and AD pathological features.

Conclusions

The present study is the first to demonstrate that DTI can detect differences in brain tissue in which Aβ plaques and tau pathology are present in the absence of significant neuron loss in a region central to AD pathology, the hippocampus, although more research is needed to appreciate fully how AD-related neuropathology is reflected in DTI metrics. Because this neuropathological profile mimics aspects of preclinical AD, the results of the present study lend support for the utility of DTI to noninvasively assist in possible early diagnosis of AD.

ACKNOWLEDGMENTS

The authors would like to thank Dr. Glenys A. Tennent for providing technical expertise and for graciously sharing the Congo red staining standard operating procedure written on behalf of the Centre for Amyloidosis & Acute Phase Proteins, Division of Medicine, Royal Free Campus, University College London. This work was supported by Research Manitoba (to BA; Postdoctoral Fellowship to WS), the St. Boniface Hospital Research Foundation (Grant Nos. 1406-3216 and 1410-3216), the Alzheimer's Society of Manitoba, and The Honourable Douglas and Patricia Everett and Royal Canadian Properties Limited Endowment Fund (Grant No. 1403-3131). BCA holds the Honourable Douglas and Patricia Everett and Royal Canadian Properties Limited Endowment Fund Chair and the Manitoba Dementia Chair (funded by the Alzheimer's Society of Manitoba and Research Manitoba) and is a research affiliate of the Centre on Aging at the University of Manitoba.

Authors' disclosures available online (http://j-alz.com/manuscript-disclosures/17-0136r1).

REFERENCES

[1] Carrillo MC, Dean RA, Nicolas F, Miller DS, Berman R, Khachaturian Z, Bain LJ, Schindler R, Knopman D, Alzheimer's Association Research Roundtable (2013) Revisiting the framework of the National Institute on Aging-Alzheimer's Association diagnostic criteria. *Alzheimers Dement* **9**, 594-601.

[2] Newell KL, Hyman BT, Growdon JH, Hedley-Whyte ET (1999) Application of the National Institute on Aging (NIA)-Reagan Institute criteria for the neuropathological diagnosis of Alzheimer disease. *J Neuropathol Exp Neurol* **58**, 1147-1155.

[3] Teipel SJ, Grothe M, Lista S, Toschi N, Garaci FG, Hampel H (2013) Relevance of magnetic resonance imaging for early detection and diagnosis of Alzheimer disease. *Med Clin North Am* **97**, 399-424.

[4] Bernard C, Helmer C, Dilharreguy B, Amieva H, Auriacombe S, Dartigues JF, Allard M, Catheline G (2014) Time course of brain volume changes in the preclinical phase of Alzheimer's disease. *Alzheimers Dement* **10**, 143-151.e1.

[5] Acosta-Cabronero J, Nestor PJ (2014) Diffusion tensor imaging in Alzheimer's disease: Insights into the limbic-diencephalic network and methodological considerations. *Front Aging Neurosci* **6**, 266.

[6] Amlien IK, Fjell AM (2014) Diffusion tensor imaging of white matter degeneration in Alzheimer's disease and mild cognitive impairment. *Neuroscience* **276**, 206-215.

[7] Dyrba M, Grothe M, Kirste T, Teipel SJ (2015) Multimodal analysis of functional and structural disconnection in Alzheimer's disease using multiple kernel SVM. *Hum Brain Mapp* **36**, 2118-2131.

[8] Scola E, Bozzali M, Agosta F, Magnani G, Franceschi M, Sormani MP, Cercignani M, Pagani E, Falautano M, Filippi M, Falini A (2010) A diffusion tensor MRI study of patients with MCI and AD with a 2-year clinical follow-up. *J Neurol Neurosurg Psychiatry* **81**, 798-805.

[9] Braak H, Braak E (1991) Neuropathological stageing of Alzheimer-related changes. *Acta Neuropathol* **82**, 239-259.

[10] Muller MJ, Greverus D, Dellani PR, Weibrich C, Wille PR, Scheurich A, Stoeter P, Fellgiebel A (2005) Functional implications of hippocampal volume and diffusivity in mild cognitive impairment. *Neuroimage* **28**, 1033-1042.

[11] Hong YJ, Yoon B, Lim SC, Shim YS, Kim JY, Ahn KJ, Han IW, Yang DW (2013) Microstructural changes in the hippocampus and posterior cingulate in mild cognitive impairment and Alzheimer's disease: A diffusion tensor imaging study. *Neurol Sci* **34**, 1215-1221.

[12] Fellgiebel A, Wille P, Muller MJ, Winterer G, Scheurich A, Vucurevic G, Schmidt LG, Stoeter P (2004) Ultrastructural hippocampal and white matter alterations in mild cognitive impairment: A diffusion tensor imaging study. *Dement Geriatr Cogn Disord* **18**, 101-108.

[13] Clerx L, Visser PJ, Verhey F, Aalten P (2012) New MRI markers for Alzheimer's disease: A meta-analysis of diffusion tensor imaging and a comparison with medial temporal lobe measurements. *J Alzheimers Dis* **29**, 405-429.

[14] Fellgiebel A, Dellani PR, Greverus D, Scheurich A, Stoeter P, Muller MJ (2006) Predicting conversion to dementia in mild cognitive impairment by volumetric and diffusivity measurements of the hippocampus. *Psychiatry Res* **146**, 283-287.

[15] Douaud G, Menke RA, Gass A, Monsch AU, Rao A, Whitcher B, Zamboni G, Matthews PM, Sollberger M, Smith S (2013) Brain microstructure reveals early abnormalities more than two years prior to clinical progression from mild cognitive impairment to Alzheimer's disease. *J Neurosci* **33**, 2147-2155.

[16] Kantarci K, Petersen RC, Boeve BF, Knopman DS, Weigand SD, O'Brien PC, Shiung MM, Smith GE, Ivnik RJ, Tangalos EG, Jack CR Jr (2005) DWI predicts future progression to Alzheimer disease in amnestic mild cognitive impairment. *Neurology* **64**, 902-904.

[17] Jung WB, Lee YM, Kim YH, Mun CW (2015) Automated classification to predict the progression of Alzheimer's disease using whole-brain volumetry and DTI. *Psychiatry Investig* **12**, 92-102.

[18] Kantarci K, Avula R, Senjem ML, Samikoglu AR, Zhang B, Weigand SD, Przybelski SA, Edmonson HA, Vemuri P, Knopman DS, Ferman TJ, Boeve BF, Petersen RC, Jack CR Jr (2010) Dementia with Lewy bodies and Alzheimer disease: Neurodegenerative patterns characterized by DTI. *Neurology* **74**, 1814-1821.

[19] Rose SE, Janke AL, Chalk JB (2008) Gray and white matter changes in Alzheimer's disease: A diffusion tensor imaging study. *J Magn Reson Imaging* **27**, 20-26.

[20] Zhang B, Xu Y, Zhu B, Kantarci K (2014) The role of diffusion tensor imaging in detecting microstructural changes in prodromal Alzheimer's disease. *CNS Neurosci Ther* **20**, 3-9.

[21] Oishi K, Mielke MM, Albert M, Lyketsos CG, Mori S (2011) DTI analyses and clinical applications in Alzheimer's disease. *J Alzheimers Dis* **26**(Suppl 3), 287-296.

[22] Song SK, Kim JH, Lin SJ, Brendza RP, Holtzman DM (2004) Diffusion tensor imaging detects age-dependent white matter changes in a transgenic mouse model with amyloid deposition. *Neurobiol Dis* **15**, 640-647.

[23] Sun SW, Song SK, Harms MP, Lin SJ, Holtzman DM, Merchant KM, Kotyk JJ (2005) Detection of age-dependent brain injury in a mouse model of brain amyloidosis associated with Alzheimer's disease using magnetic resonance diffusion tensor imaging. *Exp Neurol* **191**, 77-85.

[24] Thiessen JD, Glazner KA, Nafez S, Schellenberg AE, Buist R, Martin M, Albensi BC (2010) Histochemical visualization and diffusion MRI at 7 Tesla in the TgCRND8 transgenic model of Alzheimer's disease. *Brain Struct Funct* **215**, 29-36.

[25] Qin YY, Li MW, Zhang S, Zhang Y, Zhao LY, Lei H, Oishi K, Zhu WZ (2013) In vivo quantitative whole-brain diffusion tensor imaging analysis of APP/PS1 transgenic mice using voxel-based and atlas-based methods. *Neuroradiology* **55**, 1027-1038.

[26] Shu X, Qin YY, Zhang S, Jiang JJ, Zhang Y, Zhao LY, Shan D, Zhu WZ (2013) Voxel-based diffusion tensor imaging of an APP/PS1 mouse model of Alzheimer's disease. *Mol Neurobiol* **48**, 78-83.

[27] Fichou Y, Schiro G, Gallat FX, Laguri C, Moulin M, Combet J, Zamponi M, Hartlein M, Picart C, Mossou E, Lortat-Jacob H, Colletier JP, Tobias DJ, Weik M (2015) Hydration water mobility is enhanced around tau amyloid fibers. *Proc Natl Acad Sci U S A* **112**, 6365-6370.

[28] Billings LM, Oddo S, Green KN, McGaugh JL, LaFerla FM (2005) Intraneuronal Abeta causes the onset of early Alzheimer's disease-related cognitive deficits in transgenic mice. *Neuron* **45**, 675-688.

[29] Kastyak-Ibrahim MZ, Di Curzio DL, Buist R, Herrera SL, Albensi BC, Del Bigio MR, Martin M (2013) Neurofibrillary tangles and plaques are not accompanied by white matter pathology in aged triple transgenic-Alzheimer disease mice. *Magn Reson Imaging* **31**, 1515-1521.

[30] Oddo S, Caccamo A, Kitazawa M, Tseng BP, LaFerla FM (2003) Amyloid deposition precedes tangle formation in a triple transgenic model of Alzheimer's disease. *Neurobiol Aging* **24**, 1063-1070.

[31] Flurkey K, Currer JM, Harrison DE (2009) Appendix G: Equivalencies of human age to life phases of mice. In *The Jackson Laboratory Handbook on Genetically Standardized Mice*, Flurkey K, Currer JM, eds. The Jackson Laboratory, Bar Harbor, ME, pp. 329-331.

[32] Jones DK (2010) *Diffusion MRI*. Oxford University Press, Inc., New York.

[33] Mori S (2007) *Introduction to Diffusion Tensor Imaging*. Elsevier B.V., Oxford, UK.

[34] Veraart J, Sijbers J, Sunaert S, Leemans A, Jeurissen B (2013) Weighted linear least squares estimation of diffusion MRI parameters: Strengths, limitations, and pitfalls. *Neuroimage* **81**, 335-346.

[35] Salvador R, Pena A, Menon DK, Carpenter TA, Pickard JD, Bullmore ET (2005) Formal characterization and extension of the linearized diffusion tensor model. *Hum Brain Mapp* **24**, 144-155.

[36] Liu M, Vemuri BC, Deriche R (2013) A robust variational approach for simultaneous smoothing and estimation of DTI. *Neuroimage* **67**, 33-41.

[37] Thiessen JD, Zhang Y, Zhang H, Wang L, Buist R, Del Bigio MR, Kong J, Li XM, Martin M (2013) Quantitative MRI and ultrastructural examination of the cuprizone mouse model of demyelination. *NMR Biomed* **26**, 1562-1581.

[38] Lein ES, Hawrylycz MJ, Ao N, Ayres M, Bensinger A, Bernard A, Boe AF, Boguski MS, Brockway KS, Byrnes EJ, Chen L, Chen L, Chen TM, Chin MC, Chong J, Crook BE, Czaplinska A, Dang CN, Datta S, Dee NR, Desaki AL, Desta T, Diep E, Dolbeare TA, Donelan MJ, Dong HW, Dougherty JG, Duncan BJ, Ebbert AJ, Eichele G, Estin LK, Faber C, Facer BA, Fields R, Fischer SR, Fliss TP, Frensley C, Gates SN, Glattfelder KJ, Halverson KR, Hart MR, Hohmann JG, Howell MP, Jeung DP, Johnson RA, Karr PT, Kawal R, Kidney JM, Knapik RH, Kuan CL, Lake JH, Laramee AR, Larsen KD, Lau C, Lemon TA, Liang AJ, Liu Y, Luong LT, Michaels J, Morgan JJ, Morgan RJ, Mortrud MT, Mosqueda NF, Ng LL, Ng R, Orta GJ, Overly CC, Pak TH, Parry SE, Pathak SD, Pearson OC, Puchalski RB, Riley ZL, Rockett HR, Rowland SA, Royall JJ, Ruiz MJ, Sarno NR, Schaffnit K, Shapovalova NV, Sivisay T, Slaughterbeck CR, Smith SC, Smith KA, Smith BI, Sodt AJ, Stewart NN, Stumpf KR, Sunkin SM, Sutram M, Tam A, Teemer CD, Thaller C, Thompson CL, Varnam LR, Visel A, Whitlock RM, Wohnoutka PE, Wolkey CK, Wong VY, Wood M, Yaylaoglu MB, Young RC, Youngstrom BL, Yuan XF, Zhang B, Zwingman TA, Jones AR (2007) Genome-wide atlas of gene expression in the adult mouse brain. *Nature* **445**, 168-176.

[39] Borg J, Chereul E (2008) Differential MRI patterns of brain atrophy in double or single transgenic mice for APP and/or SOD. *J Neurosci Res* **86**, 3275-3284.

[40] Picken MM (2010) Amyloidosis-where are we now and where are we heading? *Arch Pathol Lab Med* **134**, 545-551.

[41] Puchtler H, Waldrop FS, Meloan SN (1985) A review of light, polarization and fluorescence microscopic methods for amyloid. *Appl Pathol* **3**, 5-17.

[42] Hohsfield LA, Daschil N, Oradd G, Stromberg I, Humpel C (2014) Vascular pathology of 20-month-old hypercholesterolemia mice in comparison to triple-transgenic and APPSwDI Alzheimer's disease mouse models. *Mol Cell Neurosci* **63**, 83-95.

[43] Wu Z, Yang B, Liu C, Liang G, Liu W, Pickup S, Meng Q, Tian Y, Li S, Eckenhoff MF, Wei H (2015) Long-term dantrolene treatment reduced intraneuronal amyloid in aged Alzheimer triple transgenic mice. *Alzheimer Dis Assoc Disord* **29**, 184-191.

[44] McKee AC, Carreras I, Hossain L, Ryu H, Klein WL, Oddo S, LaFerla FM, Jenkins BG, Kowall NW, Dedeoglu A (2008) Ibuprofen reduces Abeta, hyperphosphorylated tau and memory deficits in Alzheimer mice. *Brain Res* **1207**, 225-236.

[45] Blanchard J, Wanka L, Tung YC, Cardenas-Aguayo Mdel C, LaFerla FM, Iqbal K, Grundke-Iqbal I (2010) Pharmacologic reversal of neurogenic and neuroplastic abnormalities and cognitive impairments without affecting Abeta and tau pathologies in 3xTg-AD mice. *Acta Neuropathol* **120**, 605-621.

[46] Mielke MM, Kozauer NA, Chan KC, George M, Toroney J, Zerrate M, Bandeen-Roche K, Wang MC, Vanzijl P, Pekar JJ, Mori S, Lyketsos CG, Albert M (2009) Regionally-specific diffusion tensor imaging in mild cognitive impairment and Alzheimer's disease. *Neuroimage* **46**, 47-55.

[47] Ringman JM, O'Neill J, Geschwind D, Medina L, Apostolova LG, Rodriguez Y, Schaffer B, Varpetian A, Tseng B, Ortiz F, Fitten J, Cummings JL, Bartzokis G (2007) Diffusion tensor imaging in preclinical and presymptomatic carriers of familial Alzheimer's disease mutations. *Brain* **130**, 1767-1776.

[48] Bozzali M, Falini A, Franceschi M, Cercignani M, Zuffi M, Scotti G, Comi G, Filippi M (2002) White matter damage in Alzheimer's disease assessed *in vivo* using diffusion tensor magnetic resonance imaging. *J Neurol Neurosurg Psychiatry* **72**, 742-746.

[49] Duan JH, Wang HQ, Xu J, Lin X, Chen SQ, Kang Z, Yao ZB (2006) White matter damage of patients with Alzheimer's disease correlated with the decreased cognitive function. *Surg Radiol Anat* **28**, 150-156.

[50] Naggara O, Oppenheim C, Rieu D, Raoux N, Rodrigo S, Dalla Barba G, Meder JF (2006) Diffusion tensor imaging in early Alzheimer's disease. *Psychiatry Res* **146**, 243-249.

[51] Cho H, Yang DW, Shon YM, Kim BS, Kim YI, Choi YB, Lee KS, Shim YS, Yoon B, Kim W, Ahn KJ (2008) Abnormal integrity of corticocortical tracts in mild cognitive impairment: A diffusion tensor imaging study. *J Korean Med Sci* **23**, 477-483.

[52] Ding B, Chen KM, Ling HW, Zhang H, Chai WM, Li X, Wang T (2008) Diffusion tensor imaging correlates with proton magnetic resonance spectroscopy in posterior cingulate region of patients with Alzheimer's disease. *Dement Geriatr Cogn Disord* **25**, 218-225.

[53] Fellgiebel A, Schermuly I, Gerhard A, Keller I, Albrecht J, Weibrich C, Muller MJ, Stoeter P (2008) Functional relevant loss of long association fibre tracts integrity in early Alzheimer's disease. *Neuropsychologia* **46**, 1698-1706.

[54] Mori S, Zhang J (2006) Principles of diffusion tensor imaging and its applications to basic neuroscience research. *Neuron* **51**, 527-539.

[55] Pierpaoli C, Jezzard P, Basser PJ, Barnett A, Di Chiro G (1996) Diffusion tensor MR imaging of the human brain. *Radiology* **201**, 637-648.

[56] Kerbler GM, Hamlin AS, Pannek K, Kurniawan ND, Keller MD, Rose SE, Coulson EJ (2013) Diffusion-weighted magnetic resonance imaging detection of basal forebrain cholinergic degeneration in a mouse model. *Neuroimage* **66**, 133-141.

[57] Zerbi V, Kleinnijenhuis M, Fang X, Jansen D, Veltien A, Van Asten J, Timmer N, Dederen PJ, Kiliaan AJ, Heerschap A (2013) Gray and white matter degeneration revealed by diffusion in an Alzheimer mouse model. *Neurobiol Aging* **34**, 1440-1450.

[58] Muller HP, Kassubek J, Vernikouskaya I, Ludolph AC, Stiller D, Rasche V (2013) Diffusion tensor magnetic resonance imaging of the brain in APP transgenic mice: A cohort study. *PLoS One* **8**, e67630.

[59] Acosta-Cabronero J, Williams GB, Pengas G, Nestor PJ (2010) Absolute diffusivities define the landscape of white matter degeneration in Alzheimer's disease. *Brain* **133**, 529-539.

[60] Muller HP, Vernikouskaya I, Ludolph AC, Kassubek J, Rasche V (2012) Fast diffusion tensor magnetic resonance imaging of the mouse brain at ultrahigh-field: Aiming at cohort studies. *PLoS One* **7**, e53389.